Pulmonary Nodule Detection in CT Images: False Positive Reduction Using Multi-View Convolutional Networks

Arnaud Arindra Adiyoso Setio*, Francesco Ciompi, Geert Litjens, Paul Gerke, Colin Jacobs, Sarah J. van Riel, Mathilde Marie Winkler Wille, Matiullah Naqibullah, Clara I. Sánchez, and Bram van Ginneken

***Abstract*—We propose a novel Computer-Aided Detection (CAD) system for pulmonary nodules using multi-view convolutional networks (ConvNets), for which discriminative features are automatically learnt from the training data. The network is fed with nodule candidates obtained by combining three candidate detectors specifically designed for solid, subsolid, and large nodules. For each candidate, a set of 2-D patches from differently oriented planes is extracted. The proposed architecture comprises multiple streams of 2-D ConvNets, for which the outputs are combined using a dedicated fusion method to get the final classification. Data augmentation and dropout are applied to avoid overfitting. On 888 scans of the publicly available LIDC-IDRI dataset, our method reaches high detection sensitivities of 85.4% and 90.1% at 1 and 4 false positives per scan, respectively. An additional evaluation on independent datasets from the ANODE09 challenge and DLCST is performed. We showed that the proposed multi-view ConvNets is highly suited to be used for false positive reduction of a CAD system.**

***Index Terms*—Computed tomography, computer-aided detection, convolutional networks, deep learning, lung cancer, pulmonary nodule.**

I. Introduction

LUNG cancer is the leading cause of cancer death worldwide [1]. The seminal National Lung Screening Trial [2] showed a reduction of 20% in lung cancer mortality in high-risk subjects scanned with low-dose Computed Tomography (CT), compared to the control group that received chest radiography. As a consequence of this result, lung cancer screening programs with low-dose CT imaging are being implemented in the US. Currently, only 15% of all diagnosed lung cancers are detected at an early stage, which causes a five-year survival rate of only 16%. The aim of screening is to detect cancers in an earlier stage when curative treatment options are better.

The implementation of screening would mean a significant increase of reading effort for radiologists. Computer-Aided Detection (CAD) systems have been developed to assist radiologists in the reading process and thereby potentially making lung cancer screening more cost-effective [3]–[5]. The architecture of a CAD system typically consists of two stages: 1) nodule candidates detection and 2) false positive reduction. The aim of the first step is to detect nodule candidates at a very high sensitivity, which typically implies the presence of many false positives. Simple techniques such as double thresholding and morphological operations are often used to detect a large set of candidates [4], [5]. False positives are subsequently reduced in a second stage, which determine most of the performance of CAD systems. Typically, a large set of dedicated features set is extracted and a supervised classification scheme is used [3]–[5].

Although it has been shown that CAD systems improve the reading efficiency of radiologists, a considerable number of nodules remains undetected at low false positive rates, prohibiting the use of CAD in clinical practice [6], [7]. Fig. 1 illustrates that nodules come with a wide variation in shapes, sizes, and types (e.g., solid, subsolid, calcified, pleural, etc.). In addition, the number of nodules from different categories are highly imbalanced and many irregular lesions that are visible in CT are not nodules. As a consequence, extracting underlying characteristics of nodules is difficult and requires many heuristic steps. Techniques to detect lesions with a broad spectrum of appearances are needed to improve the performance of CAD systems.

In the last years, spurred by to the large amount of available data and computational power of modern-day computers, convolutional networks (ConvNets) [8], [9] have been shown to outperform the state-of-the-art in several computer vision applications [10]–[13]. ConvNets have also been introduced in the field of medical image analysis [14]–[18]. Because ConvNets can be trained end-to-end in a supervised fashion while learning highly discriminative features, removing the need for handcrafting nodule descriptors, they are well suited to be used

Manuscript received December 15, 2015; revised February 22, 2016; accepted February 26, 2016. Date of publication March 01, 2016; date of current version April 29, 2016. This project was funded by a research grant from the Netherlands Organization for Scientific Research, Project 639.023.207. *Asterisk indicates corresponding author.*

*A. A. A. Setio is with the Diagnostic Image Analysis Group, Department of Radiology and Nuclear Medicine, Radboud University Medical Center, 6525 GA Nijmegen, The Netherlands, (e-mail: Arnaud.ArindraAdiyoso@radboudumc.nl).

F. Ciompi, G. Litjens, P. Gerke, C. Jacobs, S. J. van Riel, and C. I. Sánchez are with the Diagnostic Image Analysis Group, Department of Radiology and Nuclear Medicine, Radboud University Medical Center, 6525 GA Nijmegen, The Netherlands.

M. M. W. Wille and M. Naqibullah are with the Department of Respiratory Medicine, Gentofte Hospital, University of Copenhagen, 2900 Hellerup, Denmark.

B. van Ginneken is with the Diagnostic Image Analysis Group, Department of Radiology and Nuclear Medicine, Radboud University Medical Center, 6525 GA Nijmegen, The Netherlands, and also with Fraunhofer MEVIS, 28359 Bremen, Germany.

Color versions of one or more of the figures in this paper are available online at http://ieeexplore.ieee.org.

Digital Object Identifier 10.1109/TMI.2016.2536809

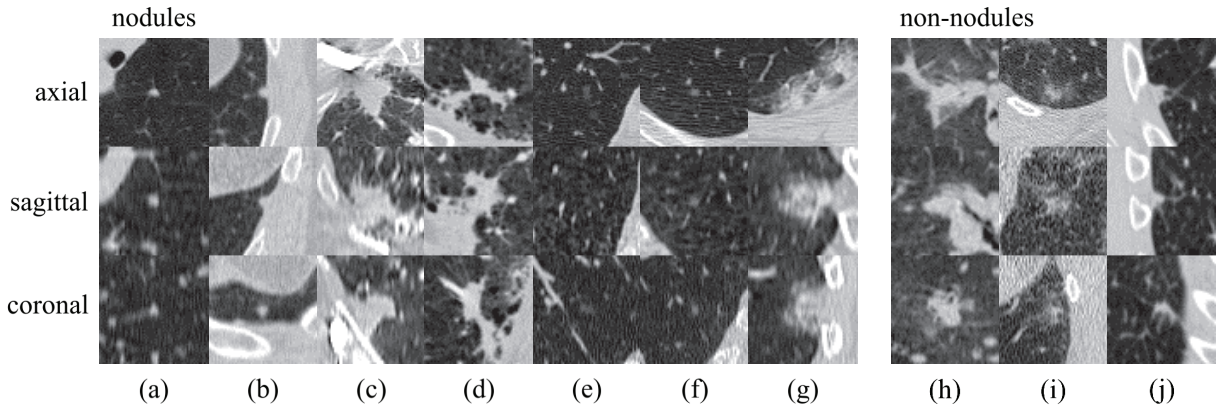

Fig. 1. Examples of lesions (nodules and non-nodules) in axial, sagittal, and coronal view. Lesions are located in the center of the box (50×50 mm). The left set of images are nodules with a wide range of morphological characteristic: (a) solid nodule, (b) pleural nodule, (c)–(d) large nodules with irregular shape, (e)–(f) subsolid nodules. The right set of images are irregular lesions that are not related with nodules or cancers. These examples illustrate that designing features for accurate detection and classification of nodules may not be trivial.

for the false positive reduction step of a pulmonary nodule CAD system. To the best of our knowledge, the work of Lo *et al.* [19] is the only study which used ConvNets specifically trained for pulmonary nodule detection, and was solely applied to chest radiography images.

Although ConvNets have been shown to outperform other supervised learning methods, only few studies extended the use of conventional 2-D ConvNets to the analysis of volumetric 3-D images [14], [17], [20]. In all these studies, volumetric candidates are firstly decomposed into fixed triplanar views (sagittal, coronal, and axial planes). Thereafter, each plane is processed using a multi-view architecture, for which streams of 2-D ConvNets are applied to all patches and output units are combined using data fusion technique, such as late-fusion [14], committee-fusion [10], [20], or the combination of both fusion methods [17]. Although all of these fusion methods show promising performance gain, how different methods compare with each other remains an open question.

The contributions of this paper are as follows: (1) We formulate a novel false positive reduction step using multi-view ConvNets for pulmonary nodule detection. Candidates are computed by combining three existing detection algorithms, which is also a contribution to boost the sensitivity of the candidate detection step. (2) We evaluated different architectures of multi-view ConvNets and their influence to the detection performance. The impact of adding more views and applying a certain fusion method on the performance of each architecture is also assessed. (3) Performance benchmark is presented and an external validation on completely independent datasets from screening trials are included.

II. Materials

A. LIDC-IDRI

We trained and validated the proposed CAD system using the large publicly available dataset, Lung Image Database Consortium (LIDC-IDRI) [21]. LIDC-IDRI contains a heterogeneous set of 1,018 cases from seven institutions. The slice thickness of CT images varies from 0.6 mm to 5.0 mm with a median of 2.0 mm. The reference standard is set by manual annotations from four radiologists who reviewed each scan in two reading rounds. In the first blinded reading round, suspicious lesions were independently annotated and each of them was categorized as non-nodule, nodule < 3 mm, or nodule ≥ 3 mm. Manual 3-D segmentation was performed only for lesions categorized as nodules ≥ 3 mm. In the second reading round, annotations from all four radiologists were reviewed in an unblinded fashion and each radiologist decided to either accept or reject each annotation.

In our study, we excluded thick-slice scans (> 2.5 mm), as these are not recommended anymore [22], [23], and scans with inconsistent slice spacing, obtaining 888 scans. We made the list of selected scans available on a public website (http://luna.grand-challenge.org/). We considered only annotations categorized as nodule ≥ 3 mm. Nodules < 3 mm are not considered relevant according to current screening protocols [2], [24]. As nodules could be annotated by multiple readers, we merged annotations that are distant less than the sum of their radii. For these merged annotations, the diameters, and coordinates were averaged. We selected nodules ≥ 3 mm accepted by the majority of radiologists (3 or 4 out of 4 radiologists) as reference standard. This resulted in a set of 1,186 nodules. Any non-nodule, nodule < 3 mm, or nodules ≥ 3 mm accepted by the minority was not counted as false positive and is considered as an irrelevant finding [6], because marks by a CAD system on such locations are not necessarily undesirable.

B. ANODE09

In order to further validate the performance of the proposed system on a dataset completely independent from the training set, we used data from the ANODE09 challenge [6]. The ANODE09 dataset consists of 55 CT scans. Each scan was annotated by two observers in a blinded fashion. Five scans were provided as training cases, while the remaining 50 cases were provided as testing cases. The reference standard for testing cases is not publicly available.

All cases were collected from the University Medical Center Utrecht and originated from a CT lung cancer screening trial

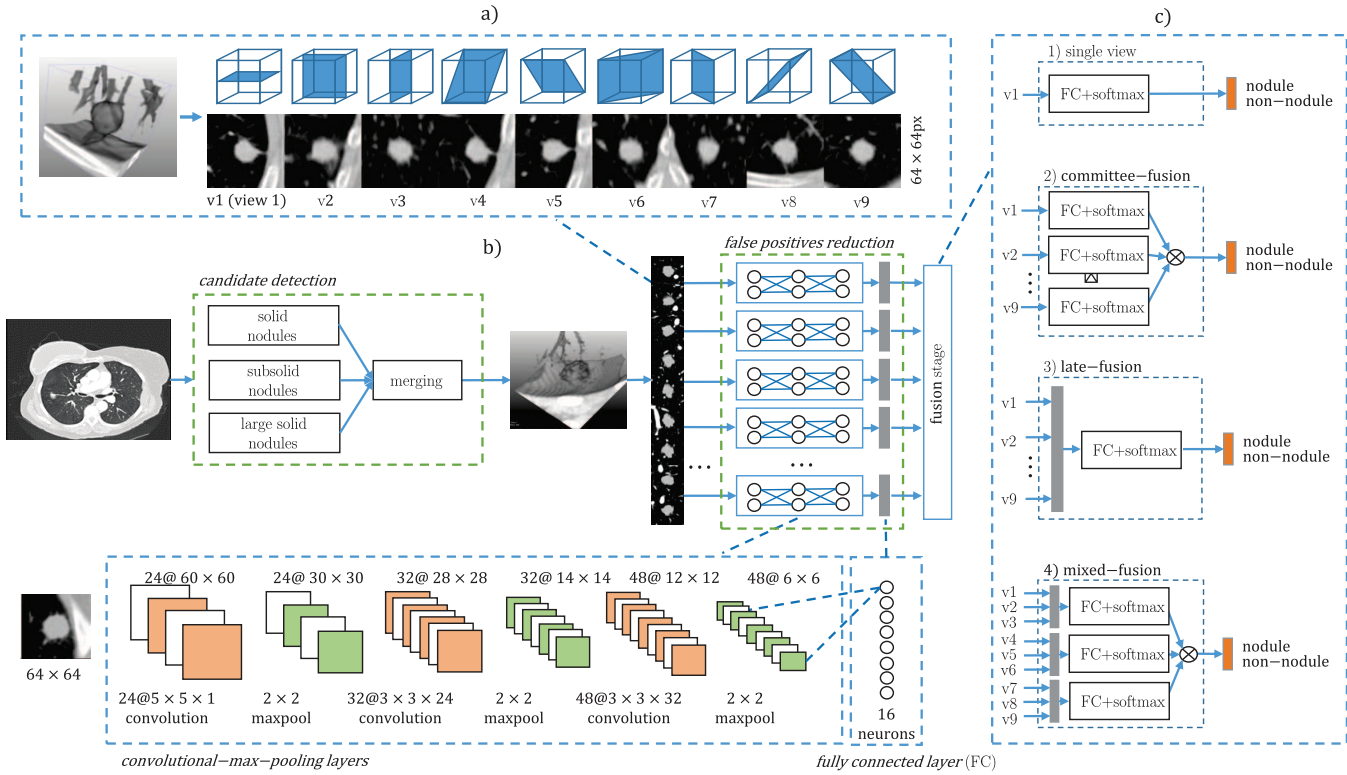

Fig. 2. An overview of the proposed CAD system. (a) An example of extracted 2-D patches from nine symmetrical planes of a cube. The candidate is located at the center of the patch with a bounding box of 50 × 50 mm and 64 × 64 px. (b) Candidates are detected by merging the outputs of detectors specifically designed for solid, subsolid and large nodules. The false positive reduction stage is implemented as a combination of multiple ConvNets. Each of the ConvNets stream processes 2-D patches extracted from a specific view. (c) Different methods for fusing the output of each ConvNet stream. Grey and orange boxes represent concatenated neurons from the first fully connected layers and the nodule classification output. Neurons are combined using fully connected layers with softmax or a fixed combiner (product-rule). (a) extracted 2-D patches using nine views of a volumetric object. (b) schematic of the proposed system. (c) fusion methods.

in Europe [24]. The images were reconstructed at 1.0 mm thickness. A web-based framework for objective evaluation of nodule detection algorithms is available[1], where the results of CAD systems can be uploaded for benchmarking.

C. DLCST

To assess the performance of the proposed nodule detection algorithm on screening setting, an evaluation on cases from the Danish Lung Cancer Screening Trial [25] was conducted. The evaluation was performed on the 612 baseline scans that were included in a recently published clinical study [26]. Nodules were annotated by 2 experienced screening radiologists of DLCST, in which the diameter was manually measured. The diameters of the two observations were averaged and positive findings were defined as nodules ≥ 3 mm. This results in a set of 898 nodules, which was used as the reference standard in this study.

III. Methods

The architecture of the proposed CAD system is schematized in Fig. 2. Two main stages are incorporated: 1) candidates detection and 2) false positive reduction. We applied three candidates detectors specifically designed for solid, subsolid, and large solid nodules. The combination of these detectors is applied to increase the detection sensitivity of nodules. Note that nodules have a large variations in both size and morphological characteristics. For each candidate, we extract multiple 2-D views in fixed planes. Each 2-D view is then processed by one ConvNets stream. The ConvNets features are then fused to compute a final score. In the next sections we describe the CAD system in details.

A. Candidates Detection

Candidate detection algorithms play an important role in the performance of any CAD system, as it determines the maximum detection sensitivity of subsequent stages. Candidate detection algorithms should ideally detect all suspicious lesions. However, the morphological variation of nodules is often greater than what a single candidate detection algorithm can detect.

To detect a wider spectrum of nodules, we applied a combination of multiple algorithms used for candidate detection. Three existing CAD systems are used to detect nodule candidates [3], [5], [27]. Each algorithm aims at a specific type of nodules, namely solid nodules, subsolid nodules, and large solid nodules. For each candidate, the position $\vec{p} = (x, y, z)$ and the nodule probability are given. Three sets of nodule candidates are computed and are merged in order to maximize the sensitivity of the detector. The candidates located closer than 5 mm to each others are merged. For these combined candidates, the position $\vec{p}$ and nodule probability are averaged [28].

[1]http://anode09.grand-challenge.org/

The methods for candidate detection stage, for which the locations of volume of interest (VOI) are obtained, are described in the following paragraphs.

For *solid* nodules, we implemented the technique proposed by Murphy *et al.* [3]. For each voxel in the lungs, shape index and curvedness are computed, and thresholding is applied on the two measures to define the seedpoints. An automatic segmentation method is executed at the seedpoints to obtain clusters of interest. Subsequently, clusters located close to each other are merged. Finally, we discard clusters with a volume $< 40\ \mathrm{mm}^3$.

For *subsolid* nodules, we implemented the technique proposed by Jacobs *et al.* [5]. A double-threshold density mask (-750, -350 Houndsfield Unit (HU)) is first performed to obtain a mask with voxels of interest. Morphological opening is applied to remove connected clusters, followed by 3D connected component analysis. Clusters for which the centers of mass are within 5 mm are merged. Finally, an accurate segmentation of the candidates is obtained by using a previously published nodule segmentation algorithm [29].

Large solid nodules ($\geq$ 10 mm) have surface/shape index values that are locally different from smaller solid lesions and have a specific intensity range that is not captured by both solid and subsolid nodules detection algorithms [27]. Therefore, the two aforementioned algorithms do not perform well in detecting large solid nodules. In addition, large solid nodules attached to the pleural wall may be excluded by lung segmentation algorithms since the contrast with the pleura is low. For these reasons, as in [27], we implemented a third detector that consists of three steps: (1) post-processing of lung segmentation by applying a rolling-ball algorithm to the segmentation mask, which includes large nodules attached to the pleura in the lung segmentation; (2) density thresholding (-300 HU), to obtain a mask with voxels of interest; (3) morphological opening in a multi-stage fashion to get candidate clusters, where we start with large structuring elements to extract larger nodules, and progressively continue with smaller structuring elements to extract smaller nodules.

One issue with training an algorithm using highly unbalanced data is that the learned parameters may be skewed toward characteristics of the most common candidates (e.g., vessels) while overlooking important characteristics of rarer nodules. To prevent overfitting on highly prevalent false positives, we discarded candidates with a low probability for being nodules. The probability was given by subsequent classification stages of existing algorithms [3], [5], [27] and the threshold is empirically set to reduce a large number of false positives while maintaining high detection sensitivity.

B. Patches Extraction

For each candidate, we extracted multiple 2-D patches of 50×50 mm centered on $\vec{p}$. The size of the patch was chosen in order to have all nodules ($\leq$ 30 mm) fully visible on the 2-D views and include sufficient context information to aid in the classification of the candidate. We resized each 50×50 mm patch to a size of 64×64 px, working at the resolution of 0.78 mm, which corresponds to the typical resolution of thin slice CT data. The pixel intensity range is rescaled from $(-1000, 400$ HU) to (0,1). Intensity outside the given range is clipped.

In order to extract patches, we first consider a cube of $50 \times 50 \times 50$ mm, which encloses the candidate. Nine patches are extracted on planes corresponding to the plane of symmetry in a cube. Similar to [14], [17], [20], three planes of symmetry that are parallel to a pair of faces of the cube are used. These planes are commonly known as sagittal, coronal, and axial planes. The other six planes are the planes of symmetry that cut two opposite faces of cubes in diagonals. Such a plane contains two opposite edges of the cube and four vertices. Examples of extracted patches are shown in Fig. 2(a).

C. False Positive Reduction: 2-D Convnets Configuration

The false positive reduction stage is constructed by combining various streams of ConvNets, referred as a multi-view architecture. Each stream processes patches from a specific view of the candidate.

The architecture of the 2-D ConvNets was determined based on a pilot study on a smaller dataset. On this dataset, several hyper-parameters (i.e., number of layers, kernel size, learning rate, number of views, fusion method) were optimized. Among these hyper-parameters, we identified two most critical parameters to tune, namely (1) the number of views and (2) the fusion method. These two parameters were further analyzed in experiments on the full selected LIDC-IDRI dataset. Other parameters were set to the best configuration found in the pilot study.

The used 2-D ConvNets consist of 3 consecutive convolutional layers and max-pooling layers (see Fig. 2(b)). The input of the network is a 64×64 patch. The first convolutional layer consists of 24 kernels of size $5 \times 5 \times 1$. The second convolutional layer consists of 32 kernels of size $3 \times 3 \times 24$. The third convolutional layer consists of 48 kernels of size $3 \times 3 \times 32$. Each kernel produces a 2-D image output (e.g., 24 of 60×60 images after the first convolutional layer, which is denoted as 24@60×60 in Fig. 2(b)). Kernels may contain different matrix values that are initialized randomly and are updated during training to optimize the classification accuracy. The max-pooling layer is given by the maximum values in non-overlapping windows of size 2×2 (stride of 2). This reduces the size of patches by half (e.g., from 24@60×60 to 24@30×30 after the first max-pooling layer). The last layer is a fully connected layer with 16 output units. Rectified linear units (ReLU) [11] are used in the convolutional layers and fully connected layers, where the activation a for a given input x is obtained as $a = \max(0, x)$.

D. False Positive Reduction: Convnets Fusion

Three approaches for fusing multiple 2-D ConvNets are investigated:

1) Committee-Fusion: One of the most commonly used fusion method is by applying a committee-based combiner to the output predictions of several ConvNets [10], [20]. The motivation is to divide the detection task of 3-D object into several simpler 2-D detection tasks. We connected the output of the fully connected layer of each stream to a classification layer that consists of an additional fully connected layer with softmax activation function. The softmax function is a multinomial logistic

regression that is given by $\sigma(\vec{x})_j = \exp(x_j)/\sum_{k=1}^{K} \exp x_k$ for $j = 1, \ldots, K$ where K is the number of classes. Each stream of ConvNets is trained separately using patches from a specific view and the output predictions are combined using a product-rule on the output probabilities [20], as shown in Fig. 2(c).

2) Late-Fusion: The late-fusion method [14], [30] concatenates the outputs of the first fully connected layers and connects the concatenated outputs directly to the classification layer (see Fig. 2(c)). With such method, the classification layer can learn the 3-D characteristics by comparing the outputs of multiple ConvNets. In this configuration, the parameters of the convolutional layers for different streams are shared.

3) Mixed-Fusion: Mixed-fusion is a combination of the previous two approaches. Similar to Roth *et al.* [17], multiple late-fused ConvNets are implemented using a fixed number of orthogonal planes. Taking an advantage of having more views, the prediction of the system is improved by combining multiple late-fused ConvNets in a committee. We divide nine patches into three independent sets; each set contains three different patches. Although other methods can be used to compose these sets of patches (e.g., random sets of triplanar patches), we attempted to compare all fusion methods fairly by keeping the same input information for each configuration.

E. Training

We performed evaluation in 5-fold cross-validation across the selected 888 LIDC-IDRI cases. We split 888 cases into 5 subsets and kept the number of candidates on each subset similar. For each fold, we used 3 subsets for training, 1 subset for validation, and 1 subset for testing. One of the challenges of using ConvNets is to efficiently optimize the weights of ConvNets given the training dataset. RMSProp [31], a learning algorithm that adaptively divide the learning rate by a running average of the magnitudes of recent gradients, is used to optimize the model. The loss is measured by using cross-entropy error and the weights are updated using mini-batches of 128 examples. Dropout [32] with a probability of 0.5 is implemented on the output of the first fully connected layer as regularization. Training is stopped when the accuracy on the validation dataset does not improve after 3 epochs. We initialized the weights using normalized initialization proposed by Glorot and Bengio [33]. The biases were initialised with zero.

F. Data Augmentation

Optimization of ConvNets using an imbalanced dataset can mislead the learning algorithm to local optima, where the predictions are biased toward the most frequent samples and overfitting occurs. Data augmentation is applied to prevent overfitting by adding invariances to the existing dataset.

1) Training Data Augmentation: As the number of nodules is much smaller than the number of non-nodules, augmentation is only performed on nodules. This process is applied for training and validation purposes. We translated the position of the candidates by 1 mm in each axis and scaled the patches to 40, 45, 50, and 55 mm. The translation is set to 1 mm in order to keep the nodules (> 3 mm) to be captured properly in the patch. We further balanced the dataset by randomly upsampling the candidates from the nodule class.

TABLE I
DETECTION SENSITIVITY OF CANDIDATE DETECTION ALGORITHMS

Total number of CT scans: 888
Total number of nodules: 1,186

Candidate detection	Detected nodules	Sensitivity (%)	False Positives (FPs)	FPs per scan
Solid	1,016	85.7	292,413	329.3
Subsolid	428	36.1	255,027	287.2
Large solid	377	31.8	41,816	47.1
Combined set	1,120	94.4	543,160	611.7
Reduced set	1,106	93.3	239,041	269.2

2) Test-Data Augmentation: Data augmentation on the testing dataset has been shown to improve the performance of ConvNets [11], [12]. It may also improve the robustness of the system as candidates are evaluated on many possible conditions, such as analyzing the input image at several scales. Test-data augmentation (TDA) is performed on each candidate (both nodule and non-nodule classes) by rescaling the patches to 40, 45, 50, and 55 mm, for which each of them is independently processed by ConvNets-CAD. We obtained the final prediction for each candidate by averaging predictions computed from the augmented data. The final prediction given by an ensemble of predictions is expected to provide complementary information and therefore make the final prediction more accurate and robust to variations of nodule size.

G. Evaluation

Two performance metrics were measured: 1) area under the ROC curve (AUC) and 2) Competition Performance Metric (CPM) [28], which measures the average sensitivity at seven operating points of the FROC curve: 1/8, 1/4, 1/2, 1, 2, 4, and 8 FPs/scan. AUC shows the performance of ConvNets on classifying candidates as nodules or non-nodules while CPM shows the performance of CAD at operating points that are likely used in practice. It has to be noted that a system with higher AUC score may not necessarily result in higher CPM. We also computed the 95% confidence interval and the p-value using bootstrapping with 1,000 bootstraps, as detailed in [34]. The p-value was defined as the probability of one performance measure to be lower than the other, where the performance measure was the detection sensitivity at 3.0 FPs/scan.

IV. EXPERIMENTAL RESULTS

A. Candidates Detection

The performance of individual candidate detection algorithms, as well as the combined algorithm is shown in Table I. When considered separately, the three approaches for solid, subsolid and large candidate detection give sensitivity of 85.7%, 36.1% and 31.8%, respectively. After the three candidate detection algorithms are combined, a sensitivity of 94.4% (1,120/1,186) is achieved. This shows that the three approaches are complementary and that combination is a better baseline for the false positive reduction. The reduced set indicates the set of candidates after removing those given a low likelihood for being nodules. The threshold is empirically set to $2.48 * 10^{-7}$,

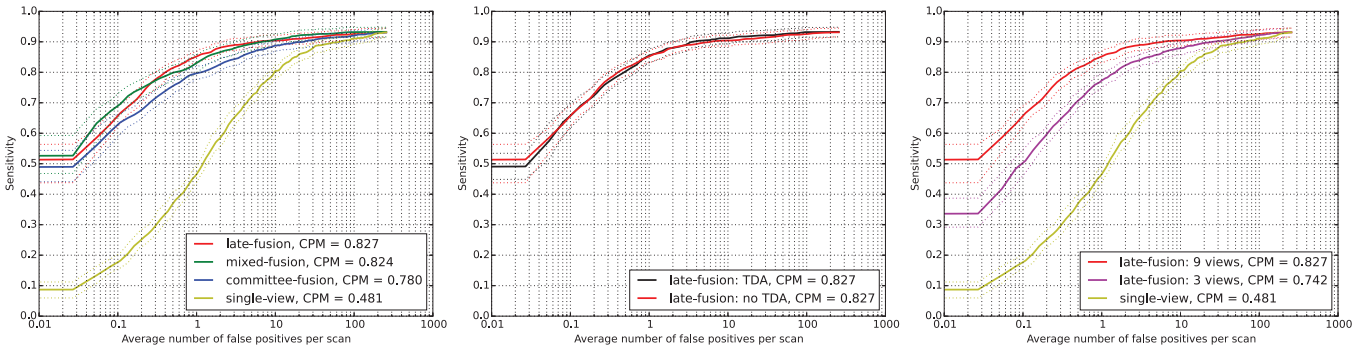

(a) (b) (c)

Fig. 3. FROC curves of ConvNets architectures with different configurations. Dashed curves show the 95% confidence interval estimated using bootstrapping. (a) different fusion configurations. (b) with and without test-data augmentation (TDA). (c) different number of views.

TABLE II
STATISTICS ON THE NUMBER OF NODULES AND NON-NODULES IN THE TRAINING DATASET. TO BALANCE THE DATASET, AUGMENTATION (AUG) AND UPSAMPLING (UP) ARE PERFORMED ON NODULES

Training dataset	Fold 0	Fold 1	Fold 2	Fold 3	Fold 4
scans	428	522	574	629	511
nodule	528	669	713	773	635
- aug	57,552	72,921	77,717	84,257	69,215
- aug+up	143,838	143,796	143,739	142,823	142,927
non-nodule	143,838	143,796	143,739	142,823	142,927

which maintains 1,106 nodules (93.25%) with 239,041 FPs (269.2 FPs/scan).

B. *False Positive Reduction*

Given a set of candidates, we constructed training datasets, which are summarized in Table II. The performance benchmark of different ConvNets configurations tested on the LIDC-IDRI dataset is summarized in Table III. Given a set of candidates, applying ConvNets for nodules/non-nodules classification task yields an area under the ROC (AUC) score up to 0.996. An average sensitivity of 0.828 at seven operating points is achieved using a late-fusion approach. We found that adding test-data augmentation does not significantly improve the detection performance (p-value $= 0.46$), as shown in Fig. 3(b). Combined with candidate detection algorithm that detect 93.1% nodules at 269.2 FPs/scan, our proposed method achieves a sensitivity of 85.4% and 90.1% at 1 and 4 FPs/scan, respectively. When irrelevant findings described in Section II-A are included as false positives, the proposed method achieves a sensitivity of 78.2% and 87.9% at 1 and 4 FPs/scan, respectively (CPM score of 0.722).

The impact of two important parameters was observed: 1) fusing model and 2) number of views. Table III shows that fully optimized fusing models (late-fusion) lead to a better detection performance with a CPM score of 0.828, in comparison with committee-fusion (CPM score of 0.780, p-value < 0.001) and mixed-fusion (CPM score of 0.823, p-value $= 0.029$).

To assess the robustness of the CAD algorithms in the presence of contrast, we also evaluated the proposed CAD on different subsets of data that consist of: 1) contrast scans (N $=$ 242) and 2) non-contrast scans (N $=$ 646). For this purpose, we trained the system with two different datasets: 1) dataset with both contrast and non-contrast scans (888 scans) and 2) dataset

TABLE III
PERFORMANCE BENCHMARK OF CONVNETS CONFIGURATIONS ON LIDC-IDRI DATASET. THE BEST SCORE FOR EACH PERFORMANCE METRIC IS MARKED IN BOLD. FOR COMPARISON PURPOSES, THE PERFORMANCE OF THE COMBINED ALGORITHMS [3], [5], [27] IS INCLUDED

Configuration	Number of views	AUC	CPM
combined algorithms	-	0.969	0.573
single-view	1	0.969	0.481
committee-fusion	3	0.981	0.696
	9	0.987	0.780
late-fusion	3	0.987	0.742
	9	0.993	**0.827**
mixed-fusion	3*3	**0.996**	0.824

TABLE IV
PERFORMANCE BENCHMARK OF CONVNETS ON CONTRAST SCANS (N $=$ 242) VS NON-CONTRAST SCANS (N $=$ 646). TWO TRAINING DATASETS ARE CONSIDERED: 1) BOTH CONTRAST AND NON-CONTRAST SCANS AND 2) ONLY NON-CONTRAST SCANS. CPM SCORE IS USED AS THE PERFORMANCE METRIC

Training dataset	test: contrast	test: non-contrast
all	0.847	0.818
non-contrast	0.840	0.807

TABLE V
PERFORMANCE BENCHMARK OF CAD SYSTEMS ON ANODE09 DATASET. THE PERFORMANCE OF CONVNETS-CAD USING TWO DIFFERENT SETS OF CANDIDATES ARE INCLUDED

Method	Score (CPM)
ConvNets-CAD (solid set)	**0.637**
ISICAD [3]	0.632
M5L [35]	0.619
ConvNets-CAD (reduced set)	**0.598**
lungCAM [35]	0.564
FlyerScan [4]	0.552
Pisa team [36]	0.293
Philips [6]	0.231
FujitaLab [6]	0.212

TABLE VI
SUMMARY OF RECENTLY PUBLISHED CAD SYSTEMS USING LIDC-IDRI AS DATASET. CAD SYSTEMS EVALUATED ON OTHER DATASET ARE ALSO INCLUDED FOR COMPLETENESS. NUMBER OF SCANS, REFERENCE STANDARD CRITERIA, AND NUMBER OF NODULES USED FOR VALIDATION ARE LISTED. NOTE THAT THE LIDC-IDRI DATASET HAS CHANGED OVER-TIME, WHICH PARTLY EXPLAINS WHY GROUPS HAVE USED DIFFERENT SUBSETS FOR THEIR EXPERIMENTS. THE REPORTED PERFORMANCE AT ONE OR TWO OPERATING POINTS IS PROVIDED

CAD systems	Year	# scans	slice thickness	nodules size (mm)	agreement levels	# nodules	sensitivity (%) / FPs/scan	
LIDC-IDRI dataset								
Proposed system	-	888	$\leq$2.5	$\geq$3	at least 3	1,186	90.1 / 4.0	85.4 / 1.0
LungCAM (Torres *et al.* [35])	2015	949	-	$\geq$3	at least 2	1,749	80.0 / 8.0	-
van Ginneken *et al.* [20])	2015	865	$\leq$2.5	$\geq$3	at least 3	1,147	76.0 / 4.0	73.0 / 1.0
Brown *et al.* [37]	2014	108	0.5-3	$\geq$4	at least 3	68	75.0 / 2.0	-
Choi and Choi [38]	2013	58	0.5-3	3-30	at least 1	151	95.3 / 2.3	-
Tan *et al.* [39]	2013	360	-	$\geq$3	at least 4	-	83.0 / 4.0	-
Teramoto and Fujita [40]	2013	84	0.5-3	5-20	at least 1	103	80.0 / 4.2	-
Cascio *et al.* [41]	2012	84	1.25-3	$\geq$3	at least 1	148	97.0 / 6.1	88.0 / 2.5
Guo and Li [42]	2012	85	1.25-3	$\geq$3	at least 3	111	80.0 / 7.4	75.0 / 2.8
Other datasets								
Jacobs *et al.* [5]	2014	109	1	$\geq$5	-	114	80.0 / 1.0	-
Zhao *et al.* [43]	2012	400	1.0	$\geq$3	-	151	96.7 / 1.9	-
Golosio *et al.* [44]	2009	23	1.25	$\geq$3	-	45	71.0 / 4.0	-
Murphy *et al.* [3]	2009	813	1	$\geq$3	-	1,525	80.0 / 4.2	-
Enquobahrie *et al.* [45]	2007	250	2.5	$\geq$4	-	395	94.0 / 7.1	-

with only non-contrast (646 scans). Table IV shows that the system trained with both contrast and non-contrast scans always achieves better performance, even on a dataset with only non-contrast scans.

The performance of the proposed ConvNets-CAD system in terms of Free-response Receiver Operating Characteristic (FROC) curve is depicted in Fig. 3(a). We also show a consistent improvement of the performance of ConvNets when more views are considered in the architecture, as shown in Fig. 3(c).

C. Comparison With Existing CAD

We applied the proposed CAD system on scans from completely independent ANODE09 dataset. The predictions were submitted to the ANODE09 evaluation system and performance were evaluated. Two sets of candidates were used. The first set (reduced set) contains candidates obtained by combining the candidate detection approaches described in Section III-A. The second set (solid set) contains candidates only from ISICAD [3], a subset of (solid) candidates that is used in the first set of candidates. The motivation is to evaluate if the ConvNets, which is the main contribution of our work, can achieve better performance in comparison with conventional feature extraction method, given the same candidates. We used the ConvNets with the late-fusion approach and the test-data augmentation to compute the nodule probability. Although we have shown that the usage of TDA does not significantly improve the performance in LIDC-IDRI dataset, we found that it substantially improves the detection performance when the ConvNets are applied to the independent dataset, ANODE09.

Table V shows the scores of the proposed ConvNets-CAD in comparison with other CAD systems in ANODE09. When only considering solid nodules candidates, the proposed ConvNets-CAD achieves the CPM score of 0.637, which outperforms other CAD systems. When TDA was not applied, a CPM of 0.492 was achieved using the same set of candidates. The scores of the other CAD systems are obtained either from ANODE09 website or from published articles if their scores are not available on the website [35].

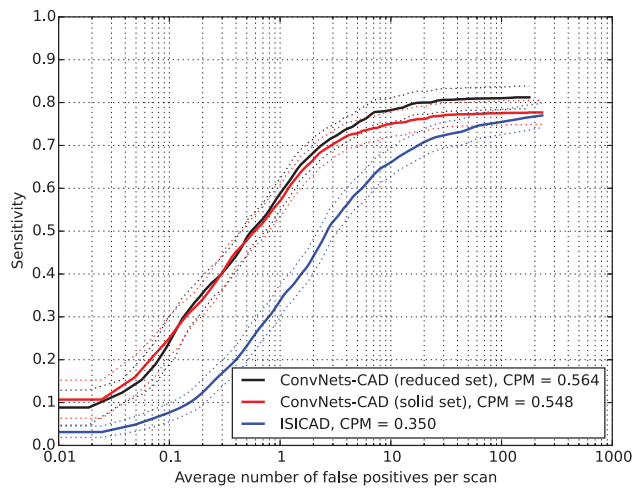

Fig. 4. FROC of CAD systems on DLCST dataset. The dataset contains 612 baseline scans with 898 annotated nodules.

To put the proposed CAD in a broader context, we reported the performance of existing CAD systems that use the LIDC-IDRI dataset for development in Table VI.

The evaluation on the independent DLCST dataset confirms that the proposed system achieves a good detection sensitivity of 76.5% at 6 FPs/scan, which is 94.0% of nodules detected by the candidate detection algorithm (Fig. 4), and outperforms the best performing CAD system in ANODE09.

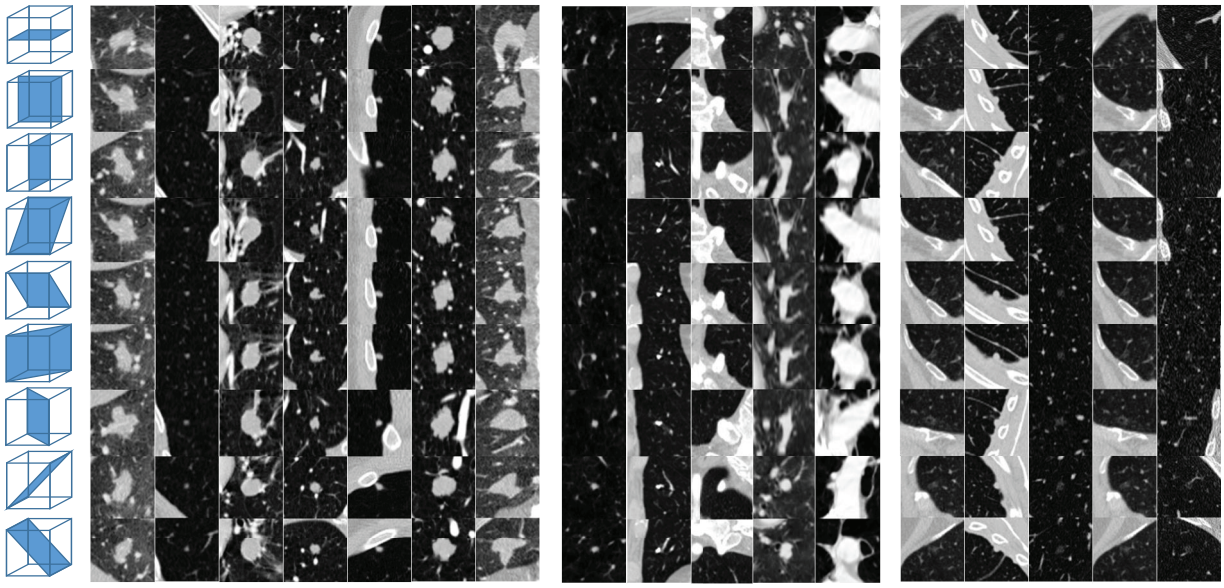

Fig. 5. Examples of lesions detected or missed by CAD system. Each column shows one lesion represented in patches viewed from different angles. The left set of lesions are nodules detected at 1 FP/scan. The middle set of lesions are false positives detected at 1 FP/scan. The right set of lesions are nodules missed at 4 FPs/scan. Most of the missed nodules are underrepresented in the current dataset.

V. Discussion

In this study, a novel pulmonary nodule detection CAD system using a multi-view convolutional network is proposed. Compared to published CAD systems that are evaluated on the publicly available LIDC-IDRI dataset, our proposed CAD system achieves comparable or better performance, indicating the potential of using ConvNets instead of using engineered features and classification as the false positive reduction stage (see Table VI). We also show that the proposed system is better than our previous CAD system that applies the off-the-shelf OverFeat network trained on million natural images of ImageNet dataset [20]. It suggests that training ConvNets specifically for the task at hand is crucial. The possibility of learning features from training dataset allows the network to learn classifying objects with a high degree of variation, which is suitable for the problem of pulmonary nodule detection.

We applied a combination of multiple candidate detection algorithms to localize suspicious lesions. Table I shows that combining multiple candidate detection algorithms boosts the detection sensitivity from 85.7% to 93.3% while maintaining a similar number of false positives.A high detection sensitivity of the candidate detection algorithm is important as it determines the upper-bound quality of the CAD system. It is worth noting that subsolid and large nodules represent a small group of nodules. However, they both add important subsets of nodules that are more likely to be cancerous.

Fig. 3(c) shows that incorporating more views in the architecture allows the network to achieve better performance. When all nine views are used, the FROC curve approaches the plateau at above 4 FPs/scan. This suggests that combining multiple views can be an effective approach for classifying 3-D objects, since simpler filters and fewer voxels are used compared to the isotropic 3-D volume ($64 \times 64 \times 64$ voxels). Following this trend, we expect that adding more views may slightly improve performance further. Experiments on different methods for fusing multiple 2-D ConvNets streams show that optimizing the combiner together with other parts of the network gives the best performance. This strategy allows the network to better learn the morphology of candidates from different perspectives, reducing errors caused by ambiguous information. As an example, vessels may be classified as nodules when the CAD system only processes one of its views. As a consequence, committee-fusion, which is commonly used in other works [10], [20], is sub-optimal for our architecture.

The evaluation on the ANODE09 dataset confirms that the proposed CAD system generalizes well on unseen data and performs accurately compared to other existing systems. When ConvNets are applied to a similar set of candidates as detected by the solid nodule detection algorithm ISICAD [3], a CPM score of 0.637 is achieved and is ranked first in ANODE09, outperforming ISICAD with a CPM score of 0.632. However, when candidates from the combined algorithm are used, the proposed system only achieves a CPM score of 0.598, outperformed by two systems: ISICAD [3] and M5L [35]. The reason for the deteriorated performance is the fact that the population of nodules on ANODE09 and that on LIDC-IDRI are different. ANODE09 dataset was randomly selected from a screening trial program to represent a screening scenario [6] while the LIDC-IDRI dataset was selected to capture the full spectrum of scans and nodules [21]. As a consequence, ANODE09 contains very few subsolid nodules and large nodules and additional candidates only contribute to more false positives. It is also worth noting that ISICAD [3], M5L [35], and lungCAM [35] were trained using a data set containing scans from the same data source of the ANODE09 study.

Additional experiments on screening cases from DLCST shows that the majority of nodules among candidates remains

correctly detected even at low FPs/scan. This shows that the proposed algorithm based on ConvNets performs consistently well as the false positive reduction step of CAD system. Although combining algorithms improves the sensitivity of the given candidate detectors, 18.7% of the annotated nodules remain undetected. Improvement of the candidate detection algorithm can substantially increase the overall performance of CAD systems, which is planned as future work.

Examples of detected nodules, false positives, and false negatives are shown in Fig. 5. Note that the system is able to detect nodules with a large variety of morphological characteristics. Fig. 5(b) shows examples of false positives. We observed that a substantial number of false positives detected at 1 FP/scan are actually nodules (first and second column) that were missed by all four radiologists. This is a problem as all nodules are required to be detected for follow-up in screening scenario. Adding CAD systems in reading processes is expected to improve the annotation of lung nodules. Osteophytes (third column), which are important for quantification of spinal abnormalities, are also found as false positives. Other typical false positives include nodular-like structures, large vessels, mediastinal structures, and scarring. At 4 FPs/scan, most of undetected nodules are subsolid nodules or nodules with irregular shape, which are underrepresented in the training set. Further data balancing on nodule categories is expected to significantly improve the performance.

The ConvNets framework is implemented using Theano [46], [47]. The computation time of ConvNets for a scan with on average 300 candidates per scan is 1 second on a standard PC with a GPU GeForce GTX TITAN X. The average training time are 315 seconds, 980 seconds, and 3,465 seconds for ConvNets with 1 view, 3 views, and 9 views, respectively.

In the context of using the CAD system for lung cancer screening, the performance in terms of sensitivity should be improved. Several suggestions are proposed for future works. Information from 3-D input data could be exploited to train the ConvNets, even though this would increase the network complexity. Another interesting direction that might also improve performance is by adding features that could not be extracted from patches (e.g., context features).

VI. Conclusion

We have presented a CAD system for pulmonary nodule detection in CT scans based on multi-view convolutional networks. We have shown that the proposed ConvNets-CAD achieves good results for the nodule detection task. The promising results and the low computation time make the ConvNets-CAD highly suited to be used as a decision aid in a lung cancer screening scenario.

Acknowledgment

The authors would like to thank the support of NVIDIA Corporation with the donation of the GPU used for this research.

References

[1] Cancer Facts and Figures 2014 Am. Cancer Soc., 2014 [Online]. Available: http://www.cancer.org/acs/groups/cid/documents/webcontent/003115-pdf.pdf

[2] D. R. Aberle *et al.*, "Reduced lung-cancer mortality with low-dose computed tomographic screening," *N. Eng. J. Med.*, vol. 365, pp. 395–409, 2011.

[3] K. Murphy, B. van Ginneken, A. M. R. Schilham, B. J. de Hoop, H. A. Gietema, and M. Prokop, "A large scale evaluation of automatic pulmonary nodule detection in chest CT using local image features and k-nearest-neighbour classification," *Med. Image Anal.*, vol. 13, pp. 757–770, 2009.

[4] T. Messay, R. C. Hardie, and S. K. Rogers, "A new computationally efficient CAD system for pulmonary nodule detection in CT imagery," *Med. Image Anal.*, vol. 14, pp. 390–406, 2010.

[5] C. Jacobs *et al.*, "Automatic detection of subsolid pulmonary nodules in thoracic computed tomography images," *Med. Image Anal.*, vol. 18, pp. 374–384, 2014.

[6] B. van Ginneken *et al.*, "Comparing and combining algorithms for computer-aided detection of pulmonary nodules in computed tomography scans: The ANODE09 study," *Med. Image Anal.*, vol. 14, pp. 707–722, 2010.

[7] M. Firmino *et al.*, "Computer-aided detection system for lung cancer in computed tomography scans: Review and future prospects," *Biomed. Eng. Online*, vol. 13, p. 41, 2014.

[8] Y. Lecun, L. Bottou, Y. Bengio, and P. Haffner, "Gradient-based learning applied to document recognition," *Proc. IEEE*, vol. 86, no. 11, pp. 2278–2324, Nov. 1998.

[9] Y. LeCun, Y. Bengio, and G. Hinton, "Deep learning," *Nature*, vol. 521, pp. 436–444, 2015.

[10] D. Cireşan, U. Meier, J. Masci, and J. Schmidhuber, "Multi-column deep neural network for traffic sign classification," *Neural Netw.*, vol. 32, pp. 333–338, 2012.

[11] A. Krizhevsky, I. Sutskever, and G. E. Hinton, "Imagenet classification with deep convolutional neural networks," *Adv. Neural Inf. Process. Syst.*, pp. 1097–1105, 2012.

[12] K. Chatfield, K. Simonyan, A. Vedaldi, and A. Zisserman, "Return of the devil in the details: Delving deep into convolutional nets," in *Br. Mach. Vis. Conf.*, 2014.

[13] K. Simonyan and A. Zisserman, Very Deep Convolutional Networks for Large-Scale Image Recognition ArXiv, 2014 [Online]. Available: arXiv:14091556

[14] A. Prasoon, K. Petersen, C. Igel, F. Lauze, E. Dam, and M. Nielsen, "Deep feature learning for knee cartilage segmentation using a triplanar convolutional neural network," in *Medical Image Computing and Computer-Assisted Intervention*. New York: Springer, 2013, vol. 8150, LNCS, pp. 246–253.

[15] A. A. Cruz-Roa, J. E. A. Ovalle, A. Madabhushi, and F. A. G. Osorio, "A deep learning architecture for image representation, visual interpretability and automated basal-cell carcinoma cancer detection," in *Medical Image Computing and Computer-Assisted Intervention*. New York: Springer, 2013, vol. 8150, LNCS, pp. 403–410.

[16] R. Li, W. Zhang, H.-I. Suk, L. Wang, J. Li, D. Shen, and S. Ji, "Deep learning based imaging data completion for improved brain disease diagnosis," in *Medical Image Computing and Computer-Assisted Intervention*. New York: Springer, 2014, vol. 8675, LNCS, pp. 305–312.

[17] H. R. Roth, L. Lu, A. Seff, K. M. Cherry, J. Hoffman, S. Wang, J. Liu, E. Turkbey, and R. M. Summers, "A new 2.5D representation for lymph node detection using random sets of deep convolutional neural network observations," in *Medical Image Computing and Computer-Assisted Intervention*. New York: Springer, 2014, vol. 8673, LNCS, pp. 520–527.

[18] T. Brosch, Y. Yoo, D. K. B. Li, A. Traboulsee, and R. Tam, "Modeling the variability in brain morphology and lesion distribution in multiple sclerosis by deep learning," in *Medical Image Computing and Computer-Assisted Intervention*. New York: Springer, 2014, vol. 8674, LNCS, pp. 462–469.

[19] S.-C. Lo *et al.*, "Artificial convolution neural network for medical image pattern recognition," *Neural Netw.*, vol. 8, pp. 1201–1214, 1995.

[20] B. van Ginneken, A. A. A. Setio, C. Jacobs, and F. Ciompi, "Off-the-shelf convolutional neural network features for pulmonary nodule detection in computed tomography scans," in *Proc. IEEE Int. Symp. Biomed. Imag.*, 2015, pp. 286–289.

[21] S. G. Armato *et al.*, "The Lung Image Database Consortium (LIDC) and Image Database Resource Initiative (IDRI): A completed reference database of lung nodules on CT scans," *Med. Phys.*, vol. 38, pp. 915–931, 2011.

[22] D. P. Naidich *et al.*, "Recommendations for the management of subsolid pulmonary nodules detected at CT: A statement from the Fleischner society," *Radiology*, vol. 266, pp. 304–317, 2013.

[23] D. Manos *et al.*, "The lung reporting and data system (LU-RADS): A proposal for computed tomography screening," *Can. Assoc. Radiol. Journ.*, vol. 65, pp. 121–134, 2014.
[24] D. M. Xu *et al.*, "Nodule management protocol of the NELSON randomised lung cancer screening trial," *Lung Cancer*, vol. 54, pp. 177–184, 2006.
[25] J. H. Pedersen *et al.*, "The Danish randomized lung cancer CT screening trial-overall design and results of the prevalence round," *J. Thoracic Oncol.*, vol. 4, pp. 608–614, 2009.
[26] M. M. W. Wille *et al.*, "Predictive accuracy of the pancan lung cancer risk prediction model -external validation based on CT from the Danish lung cancer screening trial," *Eur. Radiol.*, 2015.
[27] A. A. A. Setio, C. Jacobs, J. Gelderblom, and B. van Ginneken, "Automatic detection of large pulmonary solid nodules in thoracic CT images," *Med. Phys.*, vol. 42, no. 10, pp. 5642–5653, 2015.
[28] M. Niemeijer *et al.*, "On combining computer-aided detection systems," *IEEE Trans. Med. Imag.*, vol. 30, no. 2, pp. 215–223, Feb. 2011.
[29] J. M. Kuhnigk *et al.*, "Morphological segmentation and partial volume analysis for volumetry of solid pulmonary lesions in thoracic CT scans," *IEEE Trans. Med. Imag.*, vol. 25, no. 4, pp. 417–434, Apr. 2006.
[30] A. Karpathy, G. Toderici, S. Shetty, T. Leung, R. Sukthankar, and L. Fei-Fei, "Large-scale video classification with convolutional neural networks," in *IEEE Conf. Comput. Vis. Pattern Recognit.*, 2014, pp. 1725–1732.
[31] T. Tieleman and G. Hinton, "Lecture 6.5—RmsProp: Divide the gradient by a running average of its recent magnitude," *COURSERA: Neural Networks for Machine Learning*, 2012.
[32] N. Srivastava, G. Hinton, A. Krizhevsky, I. Sutskever, and R. Salakhutdinov, "Dropout: A simple way to prevent neural networks from overfitting," *J. Mach. Learn. Res.*, vol. 15, pp. 1929–1958, 2014.
[33] X. Glorot and Y. Bengio, "Understanding the difficulty of training deep feedforward neural networks," in *Proc. Int. Conf. Artif. Intell. Stat.*, 2010, pp. 249–256.
[34] B. Efron and R. J. Tibshirani, *An Introduction to the Bootstrap*. Boca Raton, FL: CRC Press, 1994, vol. 57.
[35] E. L. Torres *et al.*, "Large scale validation of the M5L lung CAD on heterogeneous CT datasets," *Med. Phys.*, vol. 42, pp. 1477–1489, 2015.
[36] A. Retico *et al.*, "A voxel-based neural approach (VBNA) to identify lung nodules in the ANODE09 study," *Proc. SPIE*, vol. 7260, pp. 72601S–1–72601S–8, 2009.
[37] M. S. Brown *et al.*, "Toward clinically usable CAD for lung cancer screening with computed tomography," *Eur. Radiol.*, pp. 2719–2728, 2014.
[38] W.-J. Choi and T.-S. Choi, "Automated pulmonary nodule detection system in computed tomography images: A hierarchical block classification approach," *Entropy*, vol. 15, pp. 507–523, 2013.
[39] M. Tan, R. Deklerck, J. Cornelis, and B. Jansen, "Phased searching with neat in a time-scaled framework: Experiments on a computer-aided detection system for lung nodules," *Artif. Intell. Med.*, 2013.
[40] A. Teramoto and H. Fujita, "Fast lung nodule detection in chest CT images using cylindrical nodule-enhancement filter," *Int. J. Comput. Assist. Radiol. Surg.*, pp. 1–13, 2013.
[41] D. Cascio, R. Magro, F. Fauci, M. Iacomi, and G. Raso, "Automatic detection of lung nodules in CT datasets based on stable 3D mass-spring models," *Comput. Biol. Med.*, pp. 1098–1109, 2012.
[42] W. Guo and Q. Li, "High performance lung nodule detection schemes in CT using local and global information," *Med. Phys.*, vol. 39, pp. 5157–5168, 2012.
[43] Y. Zhao *et al.*, "Performance of computer-aided detection of pulmonary nodules in low-dose CT: Comparison with double reading by nodule volume," *Eur. Radiol.*, pp. 2076–2084, 2012.
[44] B. Golosio *et al.*, "A novel multithreshold method for nodule detection in lung CT," *Med. Phys.*, vol. 36, pp. 3607–3618, 2009.
[45] A. A. Enquobahrie, A. P. Reeves, D. F. Yankelevitz, and C. I. Henschke, "Automated detection of small pulmonary nodules in whole lung CT scans," *Acad. Radiol.*, vol. 14, pp. 579–593, 2007.
[46] F. Bastien *et al.*, "Theano: New features and speed improvements," in *Deep Learning and Unsupervised Feature Learning NIPS 2012 Workshop*, 2012, pp. 1–10.
[47] J. Bergstra *et al.*, "Theano: A CPU and GPU math expression compiler," in *Proc. Python Sci. Comput. Conf.*, Jun. 2010, pp. 1–7.